Proposed Self-Limiting 2D Hexagonal Boron Nitride Growth via MOCVD for Single Photon Emitters

Robin Teng[1]

Abstract
Two-dimensional hexagonal boron nitride (2D hBN) is a critical platform for quantum nanophotonics, but its integration is severely bottlenecked by the poor crystallinity of scalable CVD films and the non-deterministic exfoliation required for pristine HPHT crystals. To resolve this, this report proposes a self-limiting Metal-Organic Chemical Vapor Deposition (MOCVD) methodology for the direct, wafer-scale synthesis of 2D hBN. Operating in the desorption-limited regime at 1000°C and 50 Torr, the process utilizes catalytic heteroepitaxy on a $Ni(111)$ substrate. This chemically anchors the initial monolayer, overcoming electrostatic preferences is expected to promote the AA stacking sequence. Concurrently, using Triethylborane (TEB) enabling the in-situ incorporation of carbon-related defect centers associated with single photon emission without post-growth annealing. By addressing these core growth mechanisms, this methodology provides a thermodynamically grounded framework for scalable synthesis of hBN for solid-state quantum photonic applications.

[1] *Department of Electrical and Computer Engineering, University of California, Santa Barbara*

Contents

1. Introduction

1.1 Bulk Hexagonal Boron Nitride

Long before its emergence in quantum optics, hexagonal boron nitride (hBN) was firmly established as an industrial workhorse in its bulk form. Characterized by an sp^2 hybridized honeycomb lattice, bulk hBN is a highly insulating dielectric with a wide indirect bandgap ($\sim$ 5.95 eV). Because it exhibits exceptional thermal and chemical stability, is completely non-wetting, and structurally robust at extreme temperatures, it has historically been utilized in heavy-duty structural applications. Currently, commercial availability of hBN is largely restricted to bulk powders used for high-temperature sintering, hot-pressed ceramics for thermal management, and pyrolytic films utilized as ultra-pure crucibles in Molecular Beam Epitaxy (MBE) systems.

1.2 hBN in the 2D Form

Following the isolation of van der Waals materials in 2004, the materials science community recognized that hBN, like graphite, can be mechanically exfoliated down to the mono-

Figure 1. Examples of bulk pyrolytic hBN crucibles utilized in high-temperature environments, such as MBE systems (Image adapted from Advanced Ceramic Materials).

layer limit. Boron nitride crystallizes in a hexagonal form at room temperature and normal pressure, serving as the most stable phase compared to its cubic and wurtzite counterparts. In this two-dimensional (2D) state, the material is quantum confined in the z-direction. Structurally, a single layer is exceptionally thin, measuring approximately 0.44 nm in thickness [1]. It consists of an alternating sheet of boron and nitrogen atoms held together by strong, sp^2 hybridized covalent bonds, establishing an in-plane lattice constant (a) of roughly 0.25 nm[cite: 53]. Conversely, multi-layer hBN relies on weak van der Waals forces in the out-of-plane (z) direction, resulting in an interlayer distance (c) of approximately 0.33 nm[cite: 62]. This atomic arrangement leaves the 2D hBN monolayer with an atomically smooth, inert surface devoid of any dangling bonds.

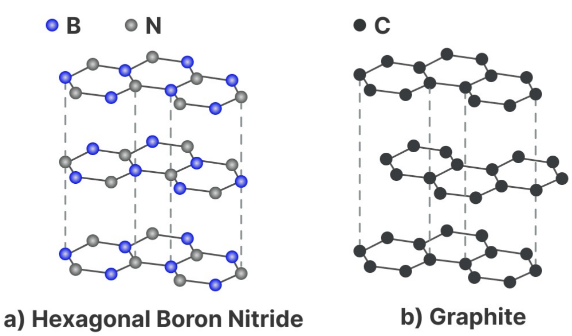

Figure 2. Structural comparison of the sp^2 hybridized honeycomb lattices of 2D hBN and graphene (Image adapted from Stanford Advanced Materials).

As shown in Figure 2, this structural similarity to graphene's hexagonal lattice has earned 2D hBN the nickname "white graphene." However, a fundamental chemical difference dictates their distinct behaviors. While graphene consists solely of a carbon atoms arranged in a honeycomb lattice, the B-N bond forms between elements of differing electronegativities. Nitrogen is significantly more electronegative than boron, pulling electron density toward itself and creating an electron dipole with partial ionic character at each B-N bond. This polar covalent bonding breaks the inversion symmetry of the lattice, making hBN a highly insulating dielectric while also dictating binding during epitaxial growth. As will be explored later in this report, this precise binding is critical for determining the interlayer stacking sequences (e.g., AA vs. AB stacking) of multi-layer films.

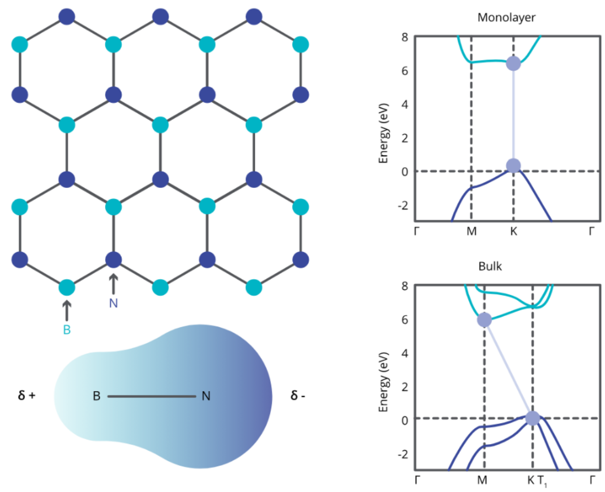

Figure 3. The 2D hBN lattice highlighting the electronegativity difference and polar covalent bonds (left), alongside the bandgap transition from bulk to monolayer (right) (Image adapted from Ossila).

Beyond its structural and electronic characteristics, the symmetry breaking and quantum confinement of 2D hBN give rise to several unique optical phenomena. As illustrated in Figure 3, as hBN approaches the monolayer limit, quantum confinement increases the bandgap compared to its bulk counterpart, ultimately transitioning the material from an indirect to a direct bandgap. As established by theoretical models developed in the Materials Department at UC Santa Barbara, this monolayer direct bandgap reaches 6.49 eV [2], driving intense UV luminescence. Furthermore, 2D hBN is a hyperbolic material[cite: 63], meaning its interaction with light is highly anisotropic and heavily dependent on the direction of propagation through the lattice. Combined with the presence of point defects capable of hosting highly stable, room-temperature single photon emitters, these optoelectronic properties makes 2D hBN a great potential platform for quantum nanophotonics.

1.3 Applications of 2D hBN

These unique structural and optical properties create a diverse application space for 2D hBN across next-generation electronics and photonics. Because the 2D surface is atomically flat and free of dangling bonds, hBN serves as an ideal dielectric encapsulation layer. It provides a pristine environment for other 2D materials, such as graphene, preventing substrate-induced scattering and preserving high carrier mobility without chemical interference.

Optically, the wide direct bandgap of 2D hBN enables efficient deep ultraviolet (DUV) emission in both monolayer and few-layer films, making it a promising candidates for next-generation DUV optoelectronics. Additionally, its inherent hyperbolic nature enables advanced nanophotonic manipulation, such as polarization splitting and the creation of "hyperlenses" capable of sub-diffraction optical imaging. Unlike traditional 3D bulk semiconductors that require strict lattice matching to a substrate, the van der Waals nature of 2D hBN allows it to be integrated seamlessly with highly disparate optical components. It can be physically transferred or grown directly onto pre-existing photonic circuits, such as silicon nitride cavities, to achieve Purcell enhancement without suffering from interfacial strain.

Most critically for the scope of this report, specific crystallographic point defects within the 2D lattice, particularly carbon-based substitutions, can function as highly stable room-temperature single photon emitters (SPEs). These defect-based quantum emitters have attracted considerable interest for emerging quantum photonic technologies and serve as a primary motivation for the controlled growth of high-quality hBN films.

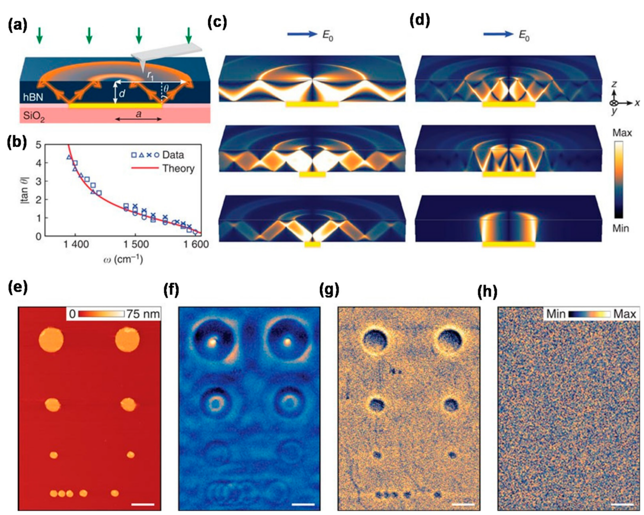

Figure 4. Experimental demonstration of sub-diffraction hyperlensing and anisotropic phonon-polariton propagation within multi-layer hBN [3].

2. Current Growth Methodologies and Bottlenecks

A variety of methods have been developed for the synthesis of hBN, including molecular beam epitaxy (MBE), physical vapor deposition (PVD), chemical vapor deposition (CVD), and high-pressure high-temperature (HPHT) growth. However, contemporary hBN research is primarily dominated by two approaches: CVD, which enables wafer-scale film growth, and HPHT synthesis, which produces high-quality bulk crystals. These methods occupy opposite ends of the scalability vs quality tradeoff and therefore serve as the primary benchmarks against which emerging growth techniques are evaluated.

2.1 Traditional Chemical Vapor Deposition

Traditional Chemical Vapor Deposition on catalytic transition metal substrates represents the primary industrial approach for large-area, continuous 2D hBN film production. This process typically relies on the vapor-phase transport of precursors, such as borazine ($B_3N_3H_6$), through a horizontal tube furnace, where they decompose over a heated metallic catalyst.

Copper (Cu) is the most heavily utilized catalytic substrate for this process, specifically because of the exceptionally low solid solubility of both boron and nitrogen within the bulk copper lattice. Unlike metals with high solubility (such as iron or nickel) where precursors dissolve into the bulk and precipitate out upon cooling, the low solubility of copper restricts the precursor decomposition strictly to a surface-mediated reaction. This surface-passivation dynamic inherently drives the growth of few-atomic-layered 2D films rather than bulk 3D precipitation. As illustrated in Figure 5, utilizing a molten copper substrate further assists the process by providing an atomically smooth surface, which reduces the density of random nucleation sites.

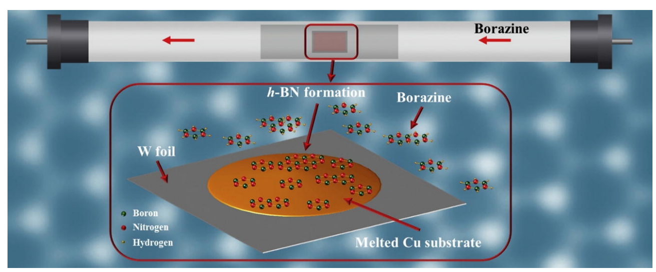

Figure 5. Schematic of a traditional horizontal CVD tube furnace utilizing borazine precursor vapor over a molten copper substrate to synthesize few-layer 2D hBN films [4].

While traditional CVD excels at generating macroscale coverage up to the wafer scale and remains highly cost-effective, it suffers from severe material quality degradation. The catalytic decomposition on standard copper foils initiates growth at thousands of random, unaligned nucleation sites across the surface. As these distinct hexagonal domains expand and coalesce, they meet at irregular angles, forming a dense network of high-angle grain boundaries, atomic vacancies, and structural dislocations.

Consequently, traditional CVD-grown hBN films are predominantly polycrystalline and exhibit a high concentration of native structural imperfections. For quantum applications, these defects are detrimental to device performance. The unregulated grain boundaries and morphological defects act as parasitic non-radiative recombination centers, which effectively quench the luminescence of single photon emitters and severely degrade the optical coherence required for quantum nanophotonics.

2.2 High-Pressure High-Temperature Synthesis

While chemical vapor deposition enables scalable hBN growth, the highest-quality hBN crystals are typically produced using High-Pressure High-Temperature (HPHT) synthesis. Pioneered at the National Institute for Materials Science (NIMS) in Japan, this growth technique has become the benchmark for producing ultra-high-purity hBN crystals used throughout the 2D materials and quantum photonics communities. In particular, crystals produced by Kenji Watanabe and Takashi Taniguchi have become widely regarded as the gold standard material for fundamental hBN research.

The HPHT process typically utilizes a seed material and dissolves a boron nitride source powder into a specialized solvent, such as a barium-boron-nitride flux, inside a sealed molybdenum crucible. This assembly is then subjected to extreme thermodynamic conditions, operating at temperatures exceeding 1500°C and immense hydrostatic pressures (upwards of 55,000 atmospheres) to force precipitation.

Achieving and sustaining these conditions requires highly specialized, cost-prohibitive equipment that is not available in standard semiconductor research facilities. One example is the 30,000-ton hydraulic press employed at NIMS, shown in Figure 6.

Figure 6. The 30,000-ton hydraulic press utilized at NIMS (Japan) for the High-Pressure High-Temperature (HPHT) synthesis of benchmark hBN crystals (Image adapted from NIMS MANA e-Bulletin) [5].

Precipitation out of this high-pressure molten flux yields single crystals with unparalleled lattice purity, chemically verified by exceptionally narrow Raman linewidths. However, while the material quality is pristine, the crystal nucleates and grows macroscopically in all directions. Because HPHT produces a bulk 3D crystal rather than a planar thin film, extracting the highly desired 2D form requires physical exfoliation, which introduces an entirely new set of critical engineering limitations.

2.3 The Exfoliation and Transfer Process

Because HPHT synthesis yields standalone, macroscopic bulk crystals, utilizing this high-quality material for two-dimensional applications requires physical thinning via mechanical exfoliation. Often referred to as the ”Scotch tape method,” this top-down approach leverages the weak out-of-plane van der Waals forces between the hBN planes to isolate individual atomic layers. As illustrated in Figure 7, the mechanical exfoliation process involves a sequential transfer: an adhesive tape is first pressed against the bulk crystal to attach the topmost layers. The tape, now carrying the layered material, is then pressed against a target substrate. Upon carefully peeling the tape away, the bottom-most layers are cleaved and left adhered to the target surface [6].

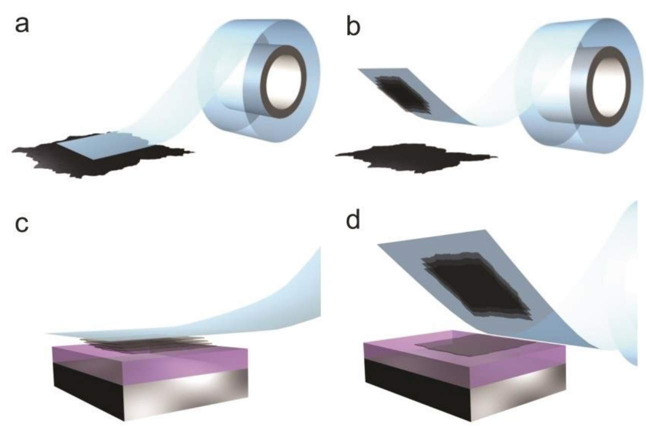

Figure 7. Step-by-step schematic of the mechanical exfoliation process utilizing adhesive tape to isolate 2D layers from a bulk crystal and transfer them to a target substrate [6].

While this top-down exfoliation technique preserves the pristine lattice quality of the parent crystal, it is entirely unscalable and non-deterministic. The resulting flakes are deposited at unpredictable locations across the substrate and exhibit little control over their geometry, with highly irregular shapes, widely varying lateral dimensions, and non-uniform layer thicknesses. As shown in Figure 8, these thickness variations manifest as distinct optical colors, while the flake boundaries remain highly irregular.

This lack of reproducibility and geometric control presents a significant challenge for scalable device fabrication. Designing practical quantum devices requires precise placement, uniform thickness, and the ability to manufacture consistent arrays. The chaotic, irreproducible nature of mechanical exfoliation renders it fundamentally unviable for large-scale manufacturing or systematic photonic integration. These limitations motivate the development of direct-growth techniques capable of producing high-quality 2D hBN films with improved control over thickness, uniformity, and device-scale integration.

3. Proposed MOCVD Growth

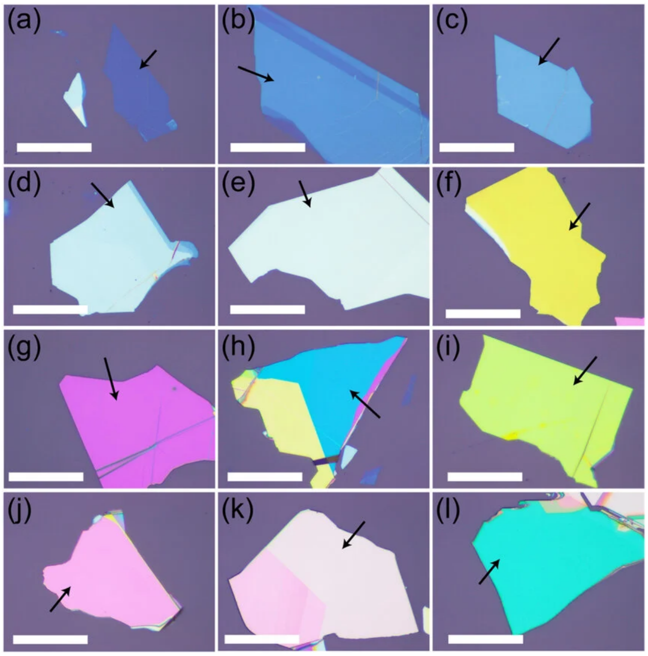

Figure 8. Optical micrograph of mechanically exfoliated hBN flakes, demonstrating the highly irregular geometries and the distinct color variations that correspond to random flake thicknesses [7].

3.1 Thermodynamic Feasibility and Phase Behavior

Before detailing the physical reactor design, it is critical to establish the thermodynamic feasibility of synthesizing high-purity hBN without the extreme pressures utilized in the NIMS process. As established previously, HPHT growth relies on high pressures and temperatures to dissolve boron nitride within a molten solvent system and subsequently precipitate high-quality crystals.

However, an analysis of the boron nitride phase diagram (Figure 9) reveals that hexagonal phase remains highly thermodynamically stable across a very wide range of low pressures and moderate temperatures. By exploiting this low-pressure stability region, vapor-phase epitaxy techniques like MOCVD can be utilized to drive highly controlled growth.

Consequently, the proposed MOCVD methodology operates at a chamber pressure of 50 Torr and a substrate temperature of 1000°C. Operating at 50 Torr increases the mean free path of the precursor species and promotes more uniform vapor transport across the substrate surface.

Although hBN remains thermodynamically stable under these conditions, achieving practical growth rates at 1000°C requires sufficient precursor decomposition and surface reaction kinetics. This is precisely where the engineering of the growth interface becomes critical. As will be detailed in the following sections, the highly catalytic nature of the chosen transition metal substrate (*Ni*) effectively bypasses the bulk thermodynamic energy barrier. The catalytic nickel surface lowers the activation energy for precursor decomposition, enabling efficient growth at temperatures that would otherwise

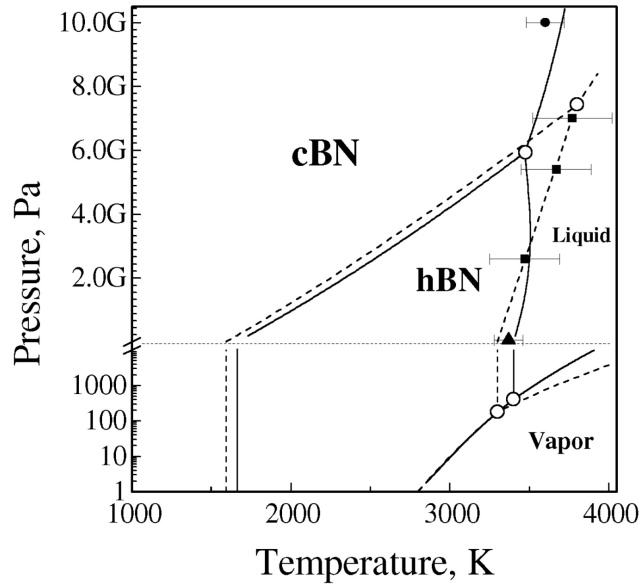

Figure 9. Phase diagram of Boron Nitride. [8].

be kinetically unfavorable.

3.2 Reactor Architecture: Vertical Stagnation Flow MOCVD

To achieve wafer-scale synthesis at the specified thermodynamic conditions, the physical reactor must be meticulously engineered to control both gas-phase fluid dynamics and thermal profiles. Traditional horizontal tube furnaces can experience precursor depletion along the gas-flow direction, often leading to non-uniform growth rates and film thicknesses. To resolve this, the proposed methodology utilizes a custom-designed vertical stagnation flow MOCVD reactor.

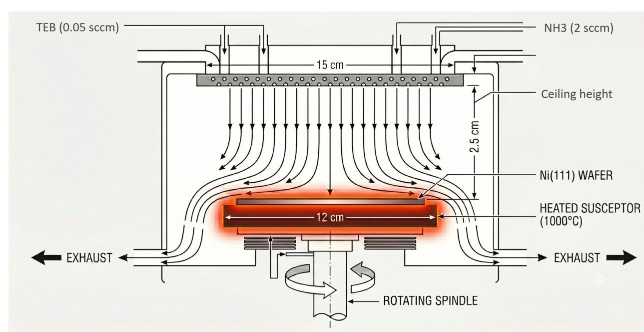

Figure 10. Cross-sectional schematic of the proposed vertical stagnation flow MOCVD reactor.

As illustrated in Figure 10, in a stagnation flow geometry, the precursor gases are injected perpendicularly downward toward the heated substrate. As the high-velocity gas stream impacts the horizontal surface, it decelerates and spreads radially outward, creating a more uniform mass transport environment across the deposition surface.

A critical vulnerability in hBN MOCVD is the tendency for Group III (boron) and Group V (nitrogen) precursors to undergo parasitic gas-phase reactions before reaching the substrate. If allowed to mix in a heated environment for too long, they will prematurely react to form solid nanoparticles (adducts) that rain down onto the film, ruining the crystal morphology. To suppress this adduct formation, the reactor is designed with two stringent thermal management features:

1. **Close-Coupled Ceiling Height:** The distance between the injection showerhead and the heated susceptor is tightly constrained to approximately 2.5 cm. This highly compressed geometry severely limits the gas residence time, forcing the precursors through the heated zone so rapidly that gas-phase adducts do not have the kinetic time to form before impacting the catalytic substrate.

2. **Water-Cooled Stainless Steel Chamber:** The outer reactor walls and the injection showerhead are constructed from stainless steel and actively water-cooled. This configuration establishes a steep thermal gradient between the heated susceptor and the cooled chamber walls. By keeping the walls cold, the precursors only reach decomposition temperatures immediately above the target substrate, strictly preventing wasteful and particle-generating parasitic deposition on the reactor walls.

To translate this highly controlled chemistry into industrial scalability, the heating stage is engineered to support a standard 4-inch (100 mm) transition metal wafer. The entire susceptor assembly continuously rotates during the growth process. This mechanical rotation averages out any microscopic spatial anomalies in the gas inlet distribution or the thermal profile, improving thickness uniformity across the wafer and reducing spatial variations in growth conditions.

3.3 Substrate Selection and AA Stacking Sequence

While the vertical MOCVD architecture provides uniform macroscopic mass transport, the growth substrate plays a critical role in determining the microscopic quality of the resulting film. To transition from the polycrystalline growth commonly observed in conventional CVD processes to highly controlled epitaxial growth, this methodology utilizes a monocrystalline Nickel (111) substrate.

As illustrated in Figure 11, the close-packed (111) facet of a face-centered cubic (fcc) nickel crystal presents a hexagonal surface geometry. Crucially, the atomic spacing of the $Ni(111)$ surface exhibits a lattice constant of $a \approx 2.49$ Å, which represents an exceptionally close lattice match to the 2.50 Å lattice constant of 2D hBN. This negligible lattice mismatch ($\sim 0.4\%$) minimizes interfacial strain and is expected to promote highly continuous epitaxial growth across large areas. Furthermore, as previously mentioned, the highly catalytic nature of the active Ni surface locally lowers the activation energy for precursor decomposition, enabling efficient growth at the 1000°C thermal limit.

Beyond promoting epitaxial growth, the choice of a $Ni(111)$ substrate may also influence the interlayer stacking sequence

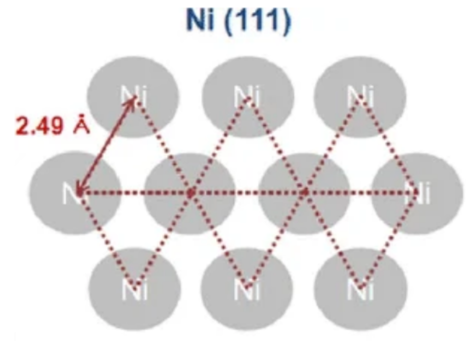

Figure 11. The hexagonal surface structre of close-packed $Ni(111)$, with an in plane lattice constant of 2.49 Å [9].

of multilayer hBN films. In multi-layer 2D materials, the specific atomic alignment between adjacent layers heavily dictates the electronic and optical properties. For hBN, there are three primary stacking configurations: AB (Bernal stacking), AA' (anti-parallel alignment), and AA (parallel alignment), as shown in Figure 12.

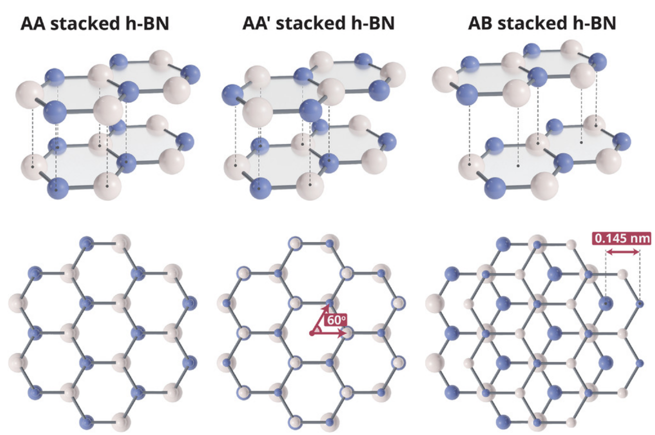

Figure 12. Structural models of the common stacking configurations in multi-layer hBN: AA, AA', and AB stacking orientations [10].

In bulk crystals synthesized via HPHT, the material naturally crystallizes in the AA' configuration. Because nitrogen is significantly more electronegative than boron, electrostatic forces dictate that the most thermodynamically stable bulk state occurs when layers alternate, placing a nitrogen atom directly above a boron atom, and vice versa. However, the restoration of inversion symmetry in AA' stacked films can limit some of the optical characteristics sought for defect-based quantum emitters. The alternating sequence restores inversion symmetry to the multi-layer structure, which alters the band structure and diminishes the efficiency of single photon emission.

Conversely, the AA stacking sequence, where boron sits directly atop boron and nitrogen atop nitrogen, preserves the broken inversion symmetry across multiple layers. This stacking arrangement has been shown to enhance interlayer quantum confinement and modify the electronic band structure relative to the naturally occurring AA' configuration. These effects are of particular interest for defect-based quantum emitters, where the local crystallographic environment plays an important role in determining optical performance.

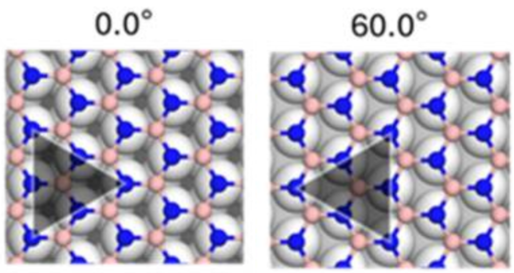

Figure 13. Atomic registry of hBN on a $Ni(111)$ surface, demonstrating how the electronegative nitrogen atoms preferentially bind to the Ni "top" sites, while boron atoms settle into the "hollow" sites.

Synthesizing the metastable AA configuration requires overcoming the natural electrostatic preference for AA' stacking. The proposed methodology leverages the specific chemical interaction between the hBN lattice and the $Ni(111)$ surface during catalytic heteroepitaxy to drive this alignment. As depicted in Figure 13, when the first monolayer of hBN nucleates on the bare nickel, the highly electronegative nitrogen atoms preferentially bind to the outermost nickel atoms (the "top" sites). Consequently, the less electronegative boron atoms tend to settle into the interstitial gaps between the nickel atoms (the fcc "hollow" sites).

This chemically driven atomic registry solidly anchors the first hBN layer to the substrate. It is anticipated that this strong interfacial bonding exerts a structural influence on subsequently deposited hBN layers. Rather than shifting into the thermodynamically favored AA' offset, the tightly bound first layer acts as a catalytic template that is expected to encourage subsequent layers to adopt a parallel alignment, thereby promoting the AA stacking sequence in few-layer films.

3.4 Precursor Chemistry and In-Situ Carbon Doping

For the MOCVD synthesis of hBN, the selection of precursor gases dictates not only the fundamental crystal stoichiometry but also the incorporation of the specific quantum-active defects necessary for photonic applications. The proposed methodology utilizes a highly purified hydrogen (H_2) carrier gas to transport the precursors into the stagnation flow boundary layer. Hydrogen is the industry standard for high-temperature epitaxy due to its excellent thermal conductivity and its reducing properties, which actively help strip away residual oxygen impurities from the growth environment.

Ammonia (NH_3) is utilized as the Group V nitrogen source. NH_3 is a well-established industrial standard for nitride-based MOCVD (such as commercial GaN and AlN synthesis). At the target susceptor temperature of $1000°C$, the NH_3 undergoes efficient catalytic cracking on the active $Ni(111)$ surface, providing a robust and continuous reactive nitrogen flux to the growth interface.

A key aspect of the proposed chemistry is the selection of Triethylborane (TEB) as the Group III boron source. While alternative boranes exist, TEB is specifically chosen for its dual-purpose capability. As established in Section 1, generating stable, room-temperature Single Photon Emitters (SPEs) associated with the carbon-based point defects within the hBN lattice. Conventionally, carbon incorporation is often achieved through post-growth techniques such as ion implantation followed by high-temperature annealing.

However, the TEB molecule inherently possesses carbon-carbon and boron-carbon bonds within its ethyl ligands. By carefully engineering the MOCVD thermal profile and the precursor flow rates, the thermal decomposition of these ethyl groups can be utilized to achieve *in-situ* carbon doping. Recent studies have demonstrated that carbon originating from TEB decomposition can be incorporated into the growing hBN lattice, providing a potential pathway toward the formation of carbon-related defect centers during growth. This eliminates the need for any secondary thermal treatments or vacuum breaks, simplifying the overall fabrication process by integrating defect incorporation directly into growth.

3.5 The Self-Limiting Growth Mechanism

The ultimate goal of this proposed methodology is not simply to grow hBN, but to achieve highly deterministic, self-limiting growth that naturally halts at the few-layer 2D limit. Achieving this requires pushing the MOCVD reactor into a highly specific thermodynamic operating window.

As illustrated in Figure 14, standard MOCVD processes are generally categorized into three temperature-dependent regimes: the reaction-rate-limited regime at low temperatures, the mass-transport-limited regime at moderate temperatures, and the desorption-limited regime at high temperatures. To prevent runaway bulk precipitation and enforce a self-limiting mechanism, this methodology intentionally operates at $1000°C$, placing the system near or within the desorption-limited growth regime.

In this regime, the overall growth rate is dictated by a strict competition between the arrival flux of the precursor molecules (adsorption) and the rate at which they boil off the surface (desorption). The self-limiting nature of this process is driven by the dynamic surface energy of the $Ni(111)$ substrate.

When the growth initiates on the bare, highly active $Ni(111)$ surface, the catalytic binding energy is extremely high. This high surface energy heavily favors adsorption, resulting in the rapid nucleation and growth of the first hBN monolayer. However, once this initial layer is completed, it effectively passivates the substrate. The catalytic influence of the underlying nickel is screened, and the binding energy available for subsequent layers is drastically reduced, relying primarily on weaker van der Waals forces.

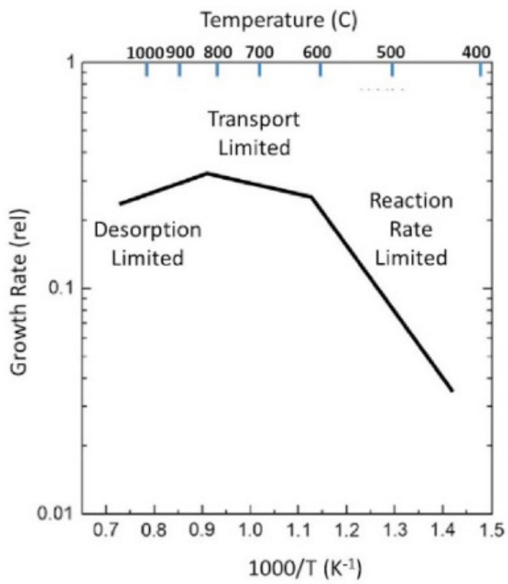

Figure 14. Generic MOCVD operating regimes as a function of temperature.

This drop in binding energy directly controls the desorption rate, which is governed by the Arrhenius equation:

$$R_{des} = A \exp\left(-\frac{E_a}{k_B T}\right) \tag{1}$$

Where R_{des} is the desorption rate, A is the pre-exponential frequency factor, E_a is the activation energy for desorption (which is strongly influenced by the layer-dependent binding energy), k_B is the Boltzmann constant, and T is the substrate temperature.

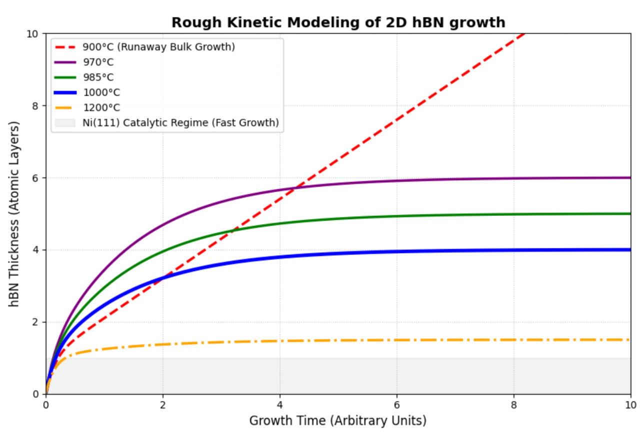

Figure 15. Expected hBN layer growth trends as a function of time and temperature. The exponential nature of the desorption kinetics allows slight thermal variations to precisely control the final equilibrium layer count.

Because the desorption rate depends exponentially on the activation energy, the reduced binding energy of successive layers can substantially increase their probability of desorption. Growth is expected to approach an equilibrium thickness when the layer-specific desorption rate strictly equals the precursor arrival flux ($R_{des} = R_{dep}$).

As demonstrated in the expected growth trend plot (Figure 15), this exponential relationship makes the system highly sensitive to the thermal budget. Because the Arrhenius function amplifies small changes in T, slight variations in the reactor temperature can be used to precisely dial in the equilibrium point. Increasing the temperature accelerates desorption, limiting the growth to a pristine monolayer, while slightly lowering the temperature allows the screened catalytic energy to support the growth of a precisely controlled few-layer film.

4. Mass Transport and Fluid Dynamics

To validate the proposed MOCVD reactor design, it is critical to quantify the fluid dynamics and mass transport behavior of the precursor gases. The reactor must maintain stable, laminar flow to ensure uniform film deposition, and the arrival flux of precursors must be precisely balanced against the thermal desorption rate to achieve self-limiting growth.

4.1 Operating & Geometry Parameters

Parameter	Symbol	Value	Unit
Reactor Pressure	P	50	Torr
Susceptor Temperature	T_s	1000 (1273)	°C (K)
Showerhead Temperature	T_u	25 (298)	°C (K)
Mean Gas Temperature	T_m	785.5	K
Ceiling Height	H_c	2.5	cm
Showerhead Diameter	D	15.0	cm
Showerhead Area	A	176.71	cm^2
Total Standard Flow	Q_0	866.67	cm^3/s
Kinematic Viscosity	ν	43.8	cm^2/s

4.2 Gas Expansion and Flow Stability

The reactor operates at a low pressure of 50 Torr and a high susceptor temperature of 1000°C. Due to these extreme conditions, the injected gases undergo significant thermal expansion as they enter the heated zone. Assuming a mean gas temperature (T_m) of 785.5 K, the ideal gas expansion multiplier (E) is calculated as:

$$E = \left(\frac{P_{STP}}{P_{Reactor}}\right)\left(\frac{T_m}{T_{STP}}\right) = \left(\frac{760}{50}\right)\left(\frac{785.5}{298}\right) = 40.06$$

This massive 40-fold volumetric expansion accelerates the total standard flow ($Q_0 = 866.67$ cm^3/s) across the 15.0 cm diameter showerhead, resulting in a true expanded inlet velocity (V_{in}) of 196.5 cm/s.

Despite this high velocity, the flow remains exceptionally stable. To verify the absence of chaotic turbulence, the

Reynolds number (Re) is calculated using the kinematic viscosity ($\nu = 43.8$ cm^2/s):

$$Re = \frac{V_{in} \cdot D}{\nu} = \frac{196.5 \cdot 15.0}{43.8} = 67.3$$

A Reynolds number of 67.3 is well below the turbulent transition threshold. Furthermore, to ensure the extreme temperature gradient between the 1000°C susceptor and the 25°C showerhead does not induce parasitic thermal convection rolls (buoyancy-driven swirling), the Rayleigh number (Ra) is evaluated:

$$Ra = \frac{\rho^2 g H_c^3 \Delta T C_p}{\eta T_m \kappa} \approx 10$$

Because $Ra \approx 10$ is drastically below the critical threshold for thermal instability (typically ~ 1708), the gas is expected to remain within a stable laminar flow regime straight down to the substrate.

4.3 Mass Transport and the Boundary Layer

As the laminar gas stream approaches the substrate, friction causes it to decelerate, forming a mass transport boundary layer (δ). Precursor molecules must diffuse across this stagnant layer to reach the catalytic surface. The thickness of this layer is:

$$\delta = 3\sqrt{\frac{\nu H_c}{V_{in}}} = 3\sqrt{\frac{43.8 \cdot 2.5}{196.5}} = 2.24 \text{ cm}$$

Crucially, this 2.24 cm boundary layer occupies nearly the entire 2.5 cm ceiling height of the reactor (H_c). This indicates that the boundary layer occupies a significant fraction of the reactor gap, suggesting that precursor transport near the substrate is strongly diffusion controlled.

The mechanism by which the Triethylborane (TEB) precursor navigates this space is defined by the Péclet number (Pe), which compares convective transport to diffusive transport:

$$Pe = Re \cdot Sc = 67.3 \cdot 1.91 = 128.5$$

With $Pe = 128.5$, convection heavily dominates the bulk gas transport pushing the precursors downward, while diffusion governs the final transport of reactants through the boundary layer to the growth surface.

4.4 Arrival Flux and Ultra-Slow Growth Rate

With the boundary layer established, the continuous precursor arrival flux ($J_{arrival}$) can be calculated. Given a TEB partial pressure (P_{TEB}) of 6.326×10^{-8} atm and a binary diffusion coefficient (D_{TEB}) of 22.93 cm^2/s, Fick's Law dictates:

$$J_{arrival} = \frac{D_{TEB} \cdot P_{TEB}}{\delta \cdot R \cdot T_m} = \frac{22.93 \cdot (6.326 \times 10^{-8})}{2.24 \cdot 82.057 \cdot 785.5} = 1.005 \times 10^{-11} \text{ mol/cm}^2\text{s}$$

Converting this molar flux into a linear physical growth rate (GR) utilizing the atomic density of the hBN lattice yields a theoretical rate of:

$$GR = 5.47 \times 10^{-4} \text{ nm/s}$$

While this translates to an exceptionally slow macroscopic growth rate, it is highly intentional and perfectly scaled for 2D materials. At an interlayer spacing of ≈ 0.33 nm, this flux equates to the deposition of approximately one hBN monolayer every 10 minutes. This intentionally low arrival flux ensures that surface kinetics govern crystal formation, rather than growth being limited by excessive precursor supply. Allowing the delicate desorption kinetics at the substrate to dictate the formation of the crystal and safely establish the self-limiting equilibrium.

4.5 Thermodynamic Proof of Self-Limiting 2D Growth

The ultimate verification of the methodology is mathematically proving that this steady arrival flux will naturally self-limit at the 2D boundary. This relies on a strict thermodynamic competition between the arrival flux ($J_{arrival}$) and the layer-dependent thermal desorption rate ($R_{des}(n)$), governed by Arrhenius kinetics:

$$R_{des}(n) = \nu_{des} \exp\left(-\frac{\Delta E_{ads}(n)}{k_B T_s}\right)$$

The adsorption binding energy (ΔE_{ads}) dictates this behavior. When growing the first layer ($n = 1$), the highly catalytic $Ni(111)$ surface creates a massive chemical binding energy ($\Delta E_{chemical}$). However, for all subsequent layers ($n > 1$), the nickel is passivated, and the layers rely on weak van der Waals forces (ΔE_{vdW}).

Because the desorption rate is exponentially sensitive to this drop in binding energy, the reactor experiences an Arrhenius "energy cliff":

$$\frac{R_{des}(n > 1)}{R_{des}(n = 1)} = \exp\left(\frac{\Delta E_{chemical} - \Delta E_{vdW}}{k_B T_s}\right) \gg 1$$

At a thermal budget of 1000°C, the desorption rate for the first layer remains effectively zero ($R_{des}(1) < J_{arrival}$), permanently anchoring the initial hBN monolayer. However, the weakened binding energy of the second layer causes its theoretical desorption rate to skyrocket until it strictly overtakes the incoming gas flux ($R_{des}(2) > J_{arrival}$). Consequently, any precursors attempting to form a second layer are immediately boiled off the surface, driving the system into thermal equilibrium and enforcing a strict, self-limiting 2D growth regime.

5. Technical Challenges and Future Outlook

While the proposed MOCVD methodology utilizing a $Ni(111)$ substrate and TEB precursor offers a compelling, thermodynamically sound pathway to scalable, AA-stacked 2D hBN, the transition from theoretical feasibility to industrial viability presents several significant engineering challenges. These hurdles span kinetic control, material interfaces, and post-growth integration.

5.1 Thermodynamic and Kinetic Sensitivities

The primary advantage of the desorption-limited regime, its self-limiting nature, is also its greatest vulnerability. Because the desorption rate is exponentially dependent on the thermal budget via the Arrhenius equation, the system is exceptionally sensitive to temperature fluctuations. Temperature non-uniformities across the wafer may shift the delicate balance between the adsorption flux and the desorption rate, leading to non-uniform layer counts across the macroscopic wafer.

Furthermore, because the reactor operates dynamically with continuous precursor arrival and departure at equilibrium, the topmost layer of the hBN film is in a state of constant flux. This continuous desorption may contribute to atomic-scale surface roughness and incomplete domain coalescence on the final layer. While implementing a post-growth ”smoothing” step, such as cutting the TEB flow and annealing the film under a pure NH_3 overpressure, may help heal surface vacancies, the efficacy of this technique in perfectly planarizing the top layer remains a challenge requiring experimental optimization.

5.2 Material Interfaces: Thermal Strain and Diffusion

Operating at 1000°C introduces severe interfacial stress during the post-growth cooling phase. There is a significant mismatch in the Coefficient of Thermal Expansion (CTE) between the $Ni(111)$ substrate and the epitaxial hBN film. As the reactor cools to room temperature, the nickel contracts at a different rate than the 2D lattice. This CTE mismatch can induce significant biaxial strain, which can manifest as localized delamination, wrinkling, or cracking of the hBN film.

Additionally, the high thermal budget poses a risk of solid-state diffusion. At 1000°C, thermally activated diffusion of nickel atoms may occur outward from the substrate and intercalate into the hBN lattice. If transition metal impurities migrate into the 2D film, they may introduce deep-level trap states capable of degrading the optical performance of the intended carbon-related quantum emitters.

5.3 Precursor Handling and Economics

From a facilities perspective, while TEB effectively eliminates the need for post-growth carbon implantation, it introduces additional logistical and safety challenges. TEB is a highly pyrophoric organometallic compound, meaning it will spontaneously ignite upon contact with atmospheric oxygen. This necessitates highly specialized, ultra-high-purity gas delivery systems, double-contained vacuum lines, and rigorous safety protocols. Consequently, the capital and operational costs associated with TEB handling are expected to exceed those of alternative boron precursors.

5.4 The Post-Growth Transfer Dilemma

Ultimately, while direct MOCVD growth solves the chaotic sizing and non-deterministic nature of mechanical exfoliation, it does not completely eliminate the transfer bottleneck for all device architectures. If the hBN must be integrated with disparate, pre-fabricated optical circuits (such as silicon nitride waveguides) rather than utilizing the nickel directly as a back-gate, the film must be removed from the $Ni(111)$ substrate.

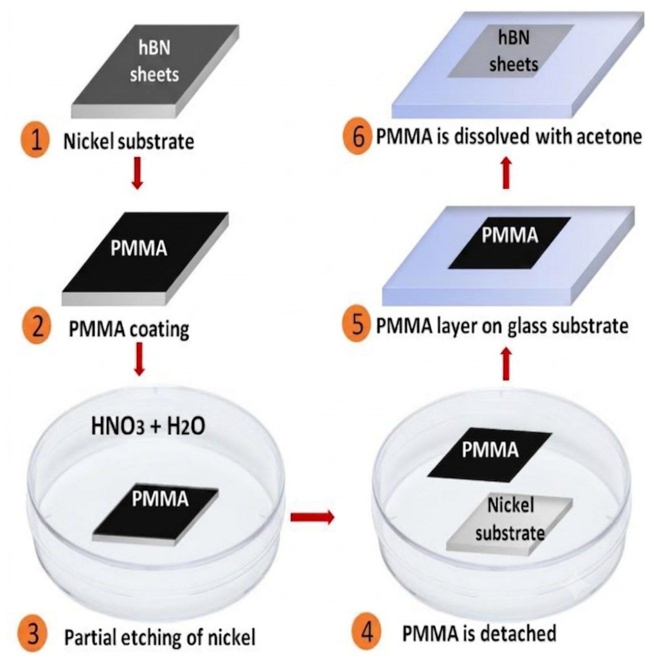

Figure 16. Schematic of the standard PMMA-assisted wet transfer process. The reliance on polymeric scaffolding and corrosive metal etchants introduces severe risks of mechanical tearing and chemical residue.

Currently, the industry standard relies on a polymer-assisted wet transfer process, utilizing Poly methyl methacrylate (PMMA). As shown in Figure 16, this involves spin-coating the hBN with PMMA, utilizing highly corrosive chemical etchants (such as iron chloride) to dissolve the underlying nickel wafer, and physically scooping the floating PMMA/hBN stack onto a new substrate. This wet transfer process can introduce a range of mechanical and chemical defects. It often leaves behind organic PMMA residues that degrade optical performance and introduces physical tears and wrinkles during the scooping phase. For this proposed MOCVD technology to become truly viable for wafer-scale quantum foundries, the development of residue-free dry-transfer techniques or direct mechanical delamination protocols will be an important area of future development.

5.5 Verification and Metrology Bottlenecks

Finally, while the proposed methodology is designed to promote AA stacking and *in-situ* carbon incorporation, experimentally verifying the resulting stacking sequence and defect chemistry remains non-trivial. High-resolution transmission electron microscopy, Raman spectroscopy, and optical characterization of individual emitters will be strictly required to confirm that the desired structural and quantum-optical properties have been achieved.

6. Conclusion

The integration of 2D hexagonal boron nitride into next-generation quantum nanophotonics is currently limited by a persistent tradeoff in materials synthesis. Traditional CVD yields scalable but highly defective polycrystalline films, while HPHT synthesis produces pristine bulk crystals that are structurally unscalable and inherently trapped behind a destructive exfoliation and transfer process.

To overcome these severe limitations, this report proposed a highly engineered Metal-Organic Chemical Vapor Deposition (MOCVD) methodology designed specifically for the direct, wafer-scale synthesis of 2D hBN for quantum photonic applications. By operating within the high-temperature desorption-limited regime (1000°C) at low pressure (50 Torr), the proposed vertical stagnation flow architecture is designed to promote deterministic, self-limiting growth at the 2D limit. Crucially, the utilization of a lattice-matched $Ni(111)$ substrate leverage catalytic heteroepitaxy to influence the natural stacking preferences of multilayer hBN, chemically anchoring the initial hBN layer and promoting the AA stacking configuration.Concurrently, the selection of Triethylborane (TEB) as a dual-purpose precursor eliminates the need for destructive post-growth annealing, enabling the *in-situ* incorporation of the carbon-based point defectsassociated with room-temperature single photon emitters.

While significant engineering challenges remain, particularly regarding thermal strain mismatch, substrate diffusion, and the continuous need for residue-free dry transfer techniques, the outlined methodology represents a thermodynamically sound pathway toward industrial manufacturability. By replacing random mechanical exfoliation with direct, self-limiting MOCVD growth, this approach could enable the transition of 2D hBN from a laboratory-scale research material to a scalable platform for quantum photonic technologies.

References

[1] Santiago J. Cartamil-Bueno et al. Mechanical characterization and cleaning of cvd single-layer h-bn resonators. *npj 2D Materials and Applications*, 1(16), 2017.

[2] Darshana Wickramaratne, Leigh Weston, and Chris G. Van de Walle. Monolayer to bulk properties of hexagonal boron nitride. *The Journal of Physical Chemistry C*, 122(44):25524–25529, 2018.

[3] S. Dai, Q. Ma, T. Andersen, A. S. Mcleod, Z. Fei, M. K. Liu, M. Wagner, K. Watanabe, T. Taniguchi, M. Thiemens, F. Keilmann, P. Jarillo-Herrero, M. M. Fogler, and D. N. Basov. Subdiffractional focusing and guiding of polaritonic rays in a natural hyperbolic material. *Nature Communications*, 6:6963, 2015.

[4] Majharul Haque Khan, Hua Kun Liu, Xudong Sun, Yusuke Yamauchi, Yoshio Bando, Dmitri Golberg, and Zhenguo Huang. Few-atomic-layered hexagonal boron nitride: Cvd growth, characterization, and applications. *Materials Today*, 20(10):611–628, 2017.

[5] National Institute for Materials Science (NIMS). Mana e-bulletin: Feature 12 - high-purity boron nitride single crystals, 2015.

[6] Victor Manuel Freire Soler. *Fabrication and Characterization of Macroscopic Graphene Layers on Metallic Substrates*. PhD thesis, Universitat Autònoma de Barcelona, 01 2014.

[7] Y. Anzai, M. Yamamoto, S. Genchi, K. Watanabe, T. Taniguchi, S. Ichikawa, Y. Fujiwara, and H. Tanaka. Broad range thickness identification of hexagonal boron nitride by colors. *Applied Physics Express*, 12(5):055007, 2019.

[8] Oleksandr O. Kurakevych and Vladimir L. Solozhenko. High-pressure design of advanced bn-based materials. *Molecules*, 21(10):1399, 2016.

[9] Daesung Jung, Cheolho Jeon, Wooseok Song, Ki-Seok An, and Chong-Yun Park. Raman spectroscopy analysis of graphene films grown on ni (111) and (100) surface. *Composites Research*, 29(4):194–202, 2016.

[10] Seokho Moon, Jiye Kim, Jeonghyeon Park, Semi Im, Jawon Kim, Inyong Hwang, and Jong Kyu Kim. Hexagonal boron nitride for next-generation photonics and electronics. *Advanced Materials*, 35(4):2204161, 2022.